Check for updates

FEBS Letters

FEBS PRESS science publishing by scientists

RESEARCH ARTICLE

The [2Fe-2S] protein CISD2 plays a key role in preventing iron accumulation in cardiomyocytes

Ola Karmi[1,2], Linda Rowland[1], Skylar D. King[1], Camila Manrique-Acevedo[3,4,5], Ioav Z. Cabantchik[2], Rachel Nechushtai[2] and Ron Mittler[1,6]

1 Department of Surgery, University of Missouri School of Medicine, Christopher S. Bond Life Sciences Center, University of Missouri, Columbia, MO, USA
2 The Alexander Silberman Institute of Life Science, The Hebrew University of Jerusalem, Israel
3 Dalton Cardiovascular Research Center, University of Missouri, Columbia, MO, USA
4 Division of Endocrinology and Metabolism, Department of Medicine, University of Missouri, Columbia, MO, USA
5 Harry S. Truman Memorial Veterans' Hospital, Columbia, MO, USA
6 The Division of Plant Sciences and Interdisciplinary Plant Group, College of Agriculture, Food and Natural Resources, Christopher S. Bond Life Sciences Center, University of Missouri, Columbia, MO, USA

Correspondence
R. Mittler, Department of Surgery, University of Missouri School of Medicine, Christopher S. Bond Life Sciences Center, University of Missouri, 1201 Rollins St, Columbia, MO 65201, USA
Tel: 1-573-882-7077
E-mail: mittlerr@missouri.edu

(Received 11 October 2021, revised 11 December 2021, accepted 30 December 2021, available online 21 January 2022)

doi:10.1002/1873-3468.14277

Edited by Barry Halliwell

Considered a key aging gene, *CISD2*, encoding CDGSH iron–sulfur domain-containing protein 2, plays a central role in regulating calcium homeostasis, preventing mitochondrial dysfunction, and the activation of autophagy and apoptosis in different cells. Here, we show that cardiomyocytes from *CISD2*-null mice accumulate high levels of iron and contain high levels of transferrin receptor and ferritin. Using proteomics and transmission electron microscopy, we further show that the lack of *CISD2* induces several features of the aging process in young mice, but other features are not induced. Taken together, our findings suggest that *CISD2* protects cardiomyocytes from overaccumulation of iron, which is common in aging hearts and can contribute to the pathogenesis of heart failure.

Keywords: cardiomyocytes; CISD2; iron; knockout mice; mitochondria; reactive oxygen species

Heart failure (HF) is one of the leading causes of death among aging individuals [1–3]. It is frequently characterized by oxidative stress-, protein misfolding-, and inflammation-associated cardiac tissue damage [4,5]. Among the most studied hallmarks of aging is mitochondrial dysfunction which is thought to cause dysregulated Ca^{2+} homeostasis, premature cell death, and metabolic inflexibility [6,7]. Because mitochondria play a key role in supporting the high energy requirements of the heart, many studies have focused on the causes of age-driven mitochondrial dysfunctions that lead to HF [8–11]. In addition to identifying reactive oxygen species (ROS), protein misfolding, and inflammation as leading drivers for HF, these studies revealed a major role for the endoplasmic reticulum (ER) and the membranes that connect the mitochondria to the ER (mitochondrial-associated membranes; MAM) in the aging process [12]. In addition, several studies demonstrated that mitochondria of aging cardiomyocytes accumulate high levels of iron that could further cause the accumulation of ROS and the induction of ferroptosis [13,14].

Abbreviations
CISD2, CDGSH iron–sulfur domain-containing protein; EMMA, European Mouse Mutant Archive; ER, endoplasmic reticulum; HF, heart failure; IHC, immunohistochemistry; KO, knockout; MAM, mitochondria–ER-associated membranes; NAF-1, nutrient-deprivation autophagy factor-1; OMM, outer mitochondrial membrane; ROS, reactive oxygen species; TEM, transmission electron microscope; TfR, transferrin receptor; WFS2, Wolfram syndrome 2.

18733468, 2022, 6, Downloaded from https://febs.onlinelibrary.wiley.com/doi/10.1002/1873-3468.14277 by CochraneChina, Wiley Online Library on [02/03/2023]. See the Terms and Conditions (https://onlinelibrary.wiley.com/terms-and-conditions) on Wiley Online Library for rules of use; OA articles are governed by the applicable Creative Commons License

Among the different proteins that reside on the cytosolic-facing surface of the mitochondria, ER, and MAM is the membrane anchored [2Fe-2S] cluster homodimeric protein CISD2 (CDGSH iron–sulfur domain-containing protein 2; also called nutrient autophagy factor 1; NAF-1) [15]. Recent studies revealed that CISD2 plays a key role in regulating Ca^{2+} homeostasis and signaling; mitochondrial iron and ROS levels; and autophagy, apoptosis, and ferroptosis in various cell types [16,17]. Mutations in *CISD2* cause Wolfram Syndrome 2 (WFS2), a rare genetic disease characterized by early diabetes mellitus, neurodegeneration, and many other symptoms that lead to a shortened life span [18–23]. Studies of *CISD2*-null and overexpressing mice identified *CISD2* as a key aging gene [17,24–26], and analysis of CISD2 levels in human heart tissues revealed that with aging, the levels of CISD2 decline [17,27]. A detailed study of *CISD2* function in the mouse heart found that the lack of *CISD2* results in dysregulation of sarco/endoplasmic reticulum Ca^{2+}-ATPase activity, causing increased levels of basal cytosolic Ca^{2+}, mitochondrial Ca^{2+} overload, and impaired electromechanical functioning [27]. Strikingly, a mouse model of *CISD2* cardiac overexpression exhibited delayed cardiac aging and attenuated age-related structural and functional defects [17,27].

In addition to *CISD2*, *CISD1* (encoding mitoNEET), another member of the CDGSH iron–sulfur domain-containing gene family, was recently shown to protect cardiomyocytes from mitochondrial dysfunction [28,29]. In contrast to *CISD2, CISD1* is primarily localized to the cytosolic-facing side of the mitochondrial membrane [15]. *CISD1* was proposed to mediate the transfer of [2Fe–2S] clusters from the mitochondria to the cytosolic [Fe–S] biosynthetic pathway [16,30,31], as well as to donate its clusters to *CISD2* [16,32]. *CISD1* was recently shown to protect cardiac cells from apoptosis and ferroptosis [28,33], and to play a key role in regulating mitochondrial metabolism associated with different neurodegenerative diseases and diabetes [16,34–36].

Because *CISD1* and *CISD2* function in several overlapping pathways that include the regulation of mitochondrial ROS, iron, and various cell death pathways [15,16,32,37], and because HF is associated with iron accumulation in the mitochondria of aging heart cells [14], we hypothesized that one of the key functions of *CISD2* in protecting the aging heart from failing is related to its role in managing mitochondrial iron and ROS levels. Here we show that cardiomyocytes of *CISD2*-null mice accumulate high levels of iron. Interestingly, although cardiomyocytes of old mice also accumulate high levels of iron, the expression of transferrin receptor (TfR), essential for iron uptake into cells, is elevated in cardiomyocytes of *CISD2*-null mice, but not old mice. Taken together, our findings suggest that *CISD2* plays a key role in preventing iron accumulation in cardiomyocytes. *CISD2* could, therefore, cooperate with *CISD1* in protecting cardiomyocytes from overaccumulation of iron.

Materials and methods

Animal models and analysis

All animals used in this study were housed under pathogen-free conditions in animal care facilities and received humane care in compliance with the Guide for the Care and Use of Laboratory Animals (https://www.ncbi.nlm.nih.gov/books/NBK54050/). All experimental procedures were approved by the Institutional Animal Care and Use Committee of the University of Missouri (https://research.missouri.edu/acqa/acuc). C57BL/6NTac-*CISD2*$^{tm1a(EUCOMM)Wtsi}$/H (*CISD2*-KO) mice were obtained from the European Mouse Mutant Archive (EMMA) repository (https://www.infrafrontier.eu/). The following primer sequences were used for genotyping mice: Common forward primer 5′-GAATATTCAATGTGTAAAGGTTTCAA-3′, Wild type reverse primer 5′-GAAAACATTTTCACTCCTTTCTTTTT 3′, and mutant reverse primer (5mut-R1) 5′-GAACTTCGGAATAGGAACTTCG-3′, which produced a wild-type band of 257 bp and a mutant band of 178 bp (Fig. S1). The physical condition, body weight, and general condition of the animals were recorded on a weekly basis, until the day of termination. Male and female C57BL/6J wild-type (Control) and *CISD2*-KO mice were euthanized at the age of 22 weeks, and female and male C57BL/6J wild-type old mice (old mice) were terminated at the age of 55 weeks. Mice were placed under anesthesia using 4% isoflurane, sacrificed, and subjected to tissue collection. Hearts were immediately extracted and measured using a ruler to determine length (distance between the upper atriums and the lower ventricular). All further analyses were conducted on samples obtained from the left ventricle of the heart (The expression of all CISD proteins in different parts of the heart is shown in Fig. S2). For immunohistochemistry (IHC) and iron staining, tissues were fixed in 4% paraformaldehyde overnight; for proteomics and protein blot analysis, samples were immediately frozen in liquid nitrogen; and for transmission electron microscopy (TEM), samples were immediately placed in a fixative as described below. Blood samples, obtained from mice at the time of sacrifice, were profiled at the Charles River Laboratories (https://www.criver.com; Table S1). These did not show significant differences between *CISD2*-KO mice and control mice.

18733468, 2022, 6, Downloaded from https://febs.onlinelibrary.wiley.com/doi/10.1002/1873-3468.14277 by CochraneChina, Wiley Online Library on [02/03/2023]. See the Terms and Conditions (https://onlinelibrary.wiley.com/terms-and-conditions) on Wiley Online Library for rules of use; OA articles are governed by the applicable Creative Commons License

Protein blots

For protein blot analyses, cardiac tissues were collected, immediately flash-frozen in liquid nitrogen, and stored at −80 °C. Cardiac tissues were lysed by grinding in 20 mM Tris pH 8.0, 150 mM NaCl, 1% Triton 100-X, 10% glycerol, 5 mM EDTA, 5 ng·mL^{-1} aprotinin, and 5 mM PMSF and kept on ice for 2 h with vortexing every 30 min. Following centrifugation at 20 000 ***g*** for 15 min, the supernatant was denatured with Laemmli sample buffer. Protein gels were loaded with equal amounts of protein, determined using the Pierce 660 nm Protein Assay (Thermo Scientific™; Cat. No. 22662) [38], and analyzed using antibodies against CISD2/NAF-1 and mitoNEET [39,40], β-actin (R&D Systems; MAB8929, Minneapolis, MN, USA) and TfR (Abcam; ab84036, Waltham, MA, USA) and Ferritin Heavy Chain (Abcam; ab65080). Goat Anti-Rabbit IgG, H & L Chain–Specific Peroxidase Conjugate (Sigma; 401315, St. Louis, MO, USA) and peroxidase-conjugated AffiniPure Goat anti-mouse IgG (H+L) (Jackson ImmunoResearch Laboratories; AB_10015289, West Grove, PA, USA) were used as secondary antibodies [38,39]. All experiments were repeated at least three times.

Iron staining and immunohistochemistry

Cardiac tissues were fixed in 4% paraformaldehyde, processed for paraffin mounting, and then sectioned. Slides prepared from each sample were subjected to iron staining or IHC [41,42]. For iron staining, Mallory's iron stain (Perls' Prussian blue) method was used [43]. Slides were deparaffinized and rehydrated with distilled water, then potassium ferrocyanide/HCL solution was added for 10 min. After washing, the slides were counterstained with Nuclear Fast Red for 5 min. For IHC, the heat-induced epitope retrieval (HIER) method was used for either the TfR or ferritin antibodies using the Diva solution from Biocare [42]. TfR or ferritin antibodies (TfR, ab84036; Ferritin Heavy Chain, ab65080; Ferritin Light Chain, ab69090) were used as primary antibodies at a ratio of 1 : 1000 and incubated for 30 min. Secondary anti-Rabbit antibody for HRP Envision (Dako, Carpinteria, CA, USA) was exposed for another 30 min. Thenchromogen Romulin Red (Biocare) was added for 10 min, and slides were counterstained with CAT Hematoxylin (Biocare) for 3 min.

Transmission electron microscopy

Unless otherwise stated, all reagents were purchased from Electron Microscopy Sciences, and all specimen preparations were performed at the Electron Microscopy Core Facility, University of Missouri (https://emc.missouri.edu/). Tissues were fixed in 2% paraformaldehyde, 2% glutaraldehyde in 100 mM sodium cacodylate buffer of pH 7.35. Tissues were then rinsed with 100 mM sodium cacodylate buffer, pH 7.35 containing 130 mM sucrose. Secondary fixation was performed using 1% osmium tetroxide (Ted Pella, Inc. Redding, CA, USA). Specimens were then incubated at 4 °C for 1 h, rinsed with cacodylate buffer, followed by rinsing in with distilled water. En bloc staining was performed using 1% aqueous uranyl acetate (4 °C overnight). A graded dehydration series was performed using ethanol at 4 °C, transitioned into acetone, and dehydrated tissues were then infiltrated with Epon resin for 24 h at room temperature and polymerized at 60 °C overnight. Sections were cut to a thickness of 75 nm using an ultramicrotome (Ultracut UCT; Leica Microsystems, Wetzlar, Germany) and a diamond knife (Diatome, Hatfield, PA, USA). Images were acquired with a JEOL JEM 1400 transmission electron microscope (JEOL, Peabody, MA, USA) at 80 kV on a Gatan Ultrascan 1000 CCD (Gatan, Inc, Pleasanton, CA, USA) as previously described [44,45].

Proteomics analysis

Proteomics analysis was conducted on heart tissues (left ventricle) obtained from six different animals (three different males and three different females) from each group (Control, *CISD2*-KO and Old mice). Tissues were subjected to protein extraction using 175 mM Tris-HCl pH 6.8, 5% SDS, 100 mM DTT, as described in Refs [46,47]. Tissues were homogenized by using a Fisher Scientific 150 hand-held homogenizer using disposable plastic probes and further heated at 65 °C for 20 min. Protein samples were precipitated with 100% of acetone, washed, resuspended in urea buffer (6 M urea, 2 M thiourea, 100 mM ammonium bicarbonate, pH 8.0), and subjected to protein quantification using Pierce 660 nm according to the manufacturer's instructions. Equal amounts of protein (25 µg) from each sample were reduced with DTT and alkylated with IAA. The samples were digested with Lys-C (1 : 50 enzyme-to-protein mass-ratio) for 3 h at 37 °C and then digested overnight with trypsin (1 : 50 enzyme-to-protein mass-ratio). The resulted peptides were cleaned up using C18 100 µL tips (Pierce), lyophilized, and resuspended in 25 µL of 5% ACN, 0.1% FA. Peptides were analyzed using a Bruker nanoElute system attached to a Bruker timsTOF-PRO mass spectrometer *via* a Bruker CaptiveSpray source (timsToF Pro; Bruker Daltonics, Billerica, MA, USA). One-microliter injections were made directly onto a 20 cm long × 75 µm inner diameter pulled-needle analytical column packed with Waters BEH-C18 (Milford, MA, USA), 1.7 µm reversed phase resin, and peptides were separated and eluted from the analytical column with a gradient of acetonitrile at 300 nL·min^{-1}. Total run time was 90 min, Initial conditions were 3% B (A: 0.1% formic acid in water, B: 99.9% acetonitrile, 0.1% formic acid), followed by 10 min ramp to 17% B, 17–25% B over 30 min, 25–37% B over 30 min, 37–80% B over 5 min, ramp back (2 min) and hold (5 min) at initial conditions. For DDA-

18733468, 2022, 6, Downloaded from https://febs.onlinelibrary.wiley.com/doi/10.1002/1873-3468.14277 by CochraneChina, Wiley Online Library on [02/03/2023]. See the Terms and Conditions (https://onlinelibrary.wiley.com/terms-and-conditions) on Wiley Online Library for rules of use; OA articles are governed by the applicable Creative Commons License

PASEF analysis, MS data were collected in the positive-ion data-dependent PASEF mode over an m/z range of 100–1700 and an ion-mobility range of 0.6–1.6 1/k0. One MS and ten PASEF frames were acquired per cycle of 1.16 s. Target MS intensity for MS was set at 10 000 counts·s^{-1} with a minimum threshold of 2000 counts·s^{-1}. An ion mobility–based rolling collision energy of 20–59 eV (1/k0 0.6–1.6) was used. An active exclusion/reconsider precursor method with release after 0.4 min was used. If the precursor (within mass width error of 0.015 m/z) was > 4× signal intensity in subsequent scans, a second MSMS spectrum was collected. Isolation width was set to 2 m/z (< 700 m/z) or 3 (800–1500 m/z). For DIA-PASEF analysis, MS data were collected in the positive-ion data-independent PASEF mode over an m/z range of 400–1200 and an ion-mobility (IM) range of 0.57–1.47 1/k0. A total of 64 DIA_PASEF windows were used (25 m/z steps and 0.18 IM steps) with two collision energies based on IM.

Proteomics data analysis

Raw DDA data were searched using MSFragger (v3.2) against the UniProt Mouse database (UniProtUP000000589, total 17058 items, released 2021/03). The following parameters were used: trypsin as digestive enzyme, two missed cleavages allowed; ±10 p.p.m. mass error on precursor, 0.1 Da mass error on MSMS fragments; carbamidomethyl-Cys fixed modification; oxidized-Met and acetylation at protein N-terminus as variable modifications. Identified proteins were filtered by peptide and protein FDR 1% and at least two spectrum counts per protein. Proteins identified in at least two samples per group were included for further quantitation analysis. The spectral library was also generated using the DDA data with MSFragger/EasyPQP (v0.1.11). DIA-NN (v1.7.15) was used to search the dia-PASEF data. The MS1 and MS2 mass accuracy were set to 10 p.p.m. Match-between-runs (MBR) was enabled. All other settings were left default. The result was filtered at 1% precursor FDR, precursor q-value < 1%, global protein q-value < 1%, and intensity of 1000. Proteomics data were deposited in Pride (https://www.ebi.ac.uk/pride/), under the following accession number: PXD028367.

Statistics

Two-way ANOVA followed by Tukey's test or one-way Welch ANOVA were used to calculate statistical significance as appropriate. GRAPHPAD PRISM 8.3.1 (San Diego, CA, USA), the R platform, and Excel were used for generating graphs. Results are presented as mean ± SD of different biological repeat averages, each conducted with three technical repeats. Differences were defined statistically significant if the probability value was equal or less than 5% ($P < 0.05$).

Results

To study the role of *CISD2* in protecting cardiomyocytes from aging, we studied 22-week-old male and female *CISD2*-null mice (*CISD2*-KO). For comparison, we used 22-week-old C57BL/6J male and female wild-type mice (control mice) and 55-week-old male and female C57BL/6J wild-type mice (old mice). As shown in Fig. 1A, both male and female *CISD2*-KO mice were smaller than control or old mice. In addition, as previously reported [27], hearts of *CISD2*-KO mice (male or female) were smaller than those of Control mice (Fig. 1B). Protein blot analyses of heart tissues revealed that the CISD2 protein was absent in *CISD2*-KO mice and lower in old mice (compared to young control mice; Fig. 1C; in agreement with previous studies [27]). In contrast to CISD2, the level of CISD1 was similar between control, *CISD2*-KO, and old mice (Fig. 1D).

To study the levels of iron in cardiomyocytes of control, *CISD2*-KO, and old mice, we used the Perls' Prussian blue iron stain method. As shown in Fig. 2, cardiomyocytes of *CISD2*-KO mice accumulated higher levels of iron than those of control mice. Interestingly, cardiomyocytes of old mice accumulated very high levels of iron that were higher than those of control or *CISD2*-KO mice (Fig. 2). Depending on the type of cell, age, and physiological condition, high levels of iron in cells are often accompanied by altered (enhanced or decreased) expression levels of TfR that plays a key role in iron uptake into cells [48]. In addition, the level of ferritin, a key iron storage protein, is typically increased in cells with high iron levels [49]. To substantiate our findings that hearts of *CISD2*-KO mice accumulate high levels of iron, we used IHC and protein blots to measure the levels of TfR and heavy-chain ferritin in cardiomyocytes of control, old mice, and *CISD2*-KO mice. As shown in Fig. 3, compared to control young mice, cardiac myocytes of *CISD2*-KO mice (young male or female) accumulated high levels of TfR and heavy-chain ferritin. In contrast, cardiac myocytes of old mice did not accumulate high levels of TfR or heavy-chain ferritin (Fig. 3).

Enhanced levels of iron in cells, as well as the lack of CISD2, can cause alterations in mitochondria and ER structures [16,27,39,50–52]. We, therefore, used transmission electron microscopy to determine structural abnormalities in cardiomyocytes from control, *CISD2*-KO, and old mice. As shown in Fig. 4A, cardiomyocytes of both old mice and *CISD2*-KO mice contained a high level of abnormal mitochondria that displayed fewer or disrupted crista and/or abnormal/fragmented shape. In contrast, while cardiomyocytes

18733468, 2022, 6, Downloaded from https://febs.onlinelibrary.wiley.com/doi/10.1002/1873-3468.14277 by CochraneChina, Wiley Online Library on [02/03/2023]. See the Terms and Conditions (https://onlinelibrary.wiley.com/terms-and-conditions) on Wiley Online Library for rules of use; OA articles are governed by the applicable Creative Commons License

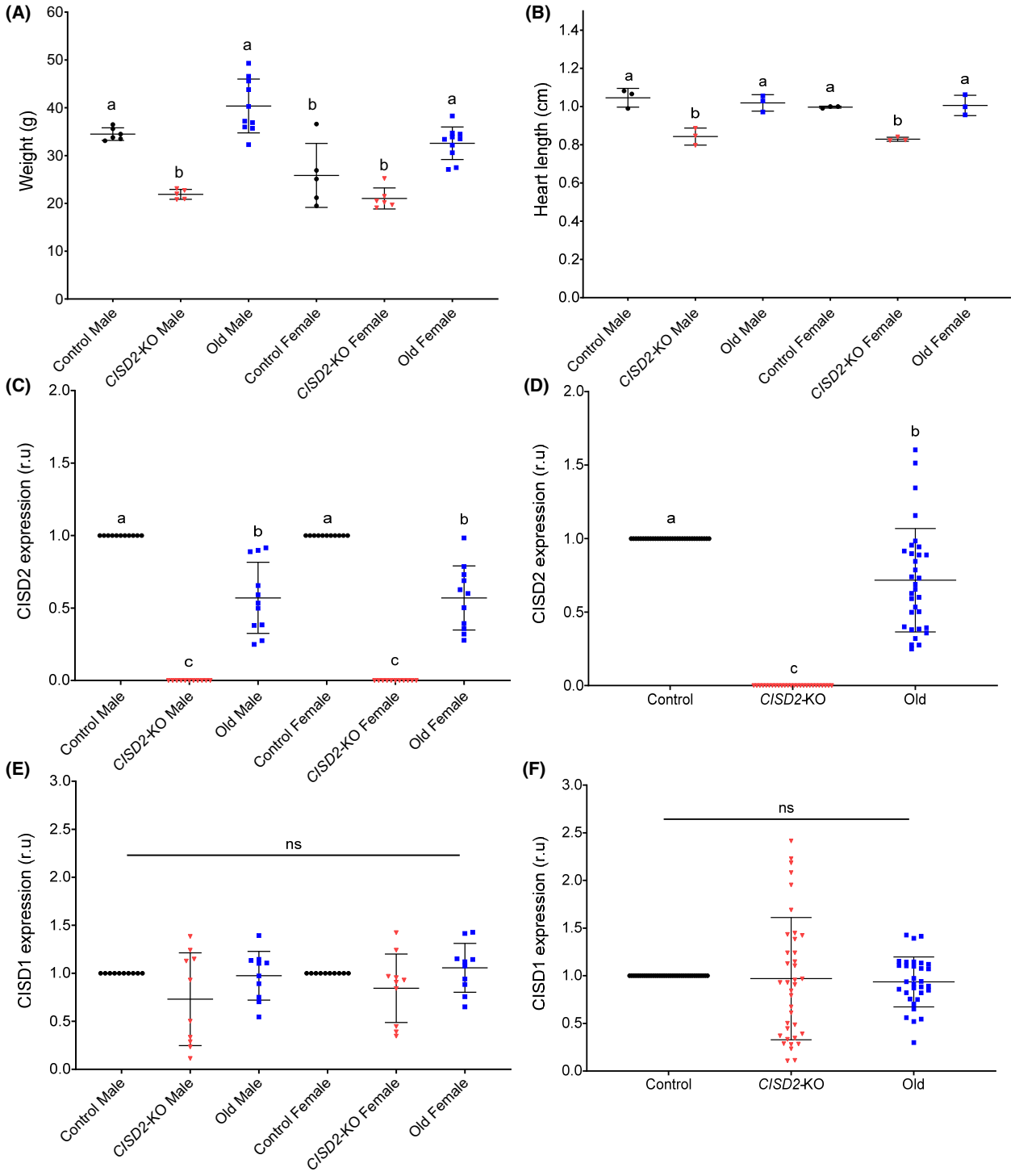


Fig. 1. Morphological and biochemical characteristics of knockout *CISD2* mice. (A) Weight (g) of control (22-week-old wild-type), *CISD2*-knockout (KO; 22-week-old *CISD2*-KO), and old (55-week-old wild-type) mice. (B) Heart length measured as distance between the upper atrium to the lower ventricle of control, *CISD2*-KO and old mice. (C–F) Protein blot analyses of CISD2 (C, D) and CISD1 (E, F) in control, *CISD2*-KO, and old mice. Results are shown for male and female separately or combined and presented as mean ± SD of six different animals (three different males and three different females) from each group (control, *CISD2*-KO, and old mice). Two-way ANOVA followed by Tukey's test were used to calculate statistical significance (ns, not significant). Lowercase letters donate significance ($P < 0.05$).

18733468, 2022, 6, Downloaded from https://febs.onlinelibrary.wiley.com/doi/10.1002/1873-3468.14277 by CochraneChina, Wiley Online Library on [02/03/2023]. See the Terms and Conditions (https://onlinelibrary.wiley.com/terms-and-conditions) on Wiley Online Library for rules of use; OA articles are governed by the applicable Creative Commons License

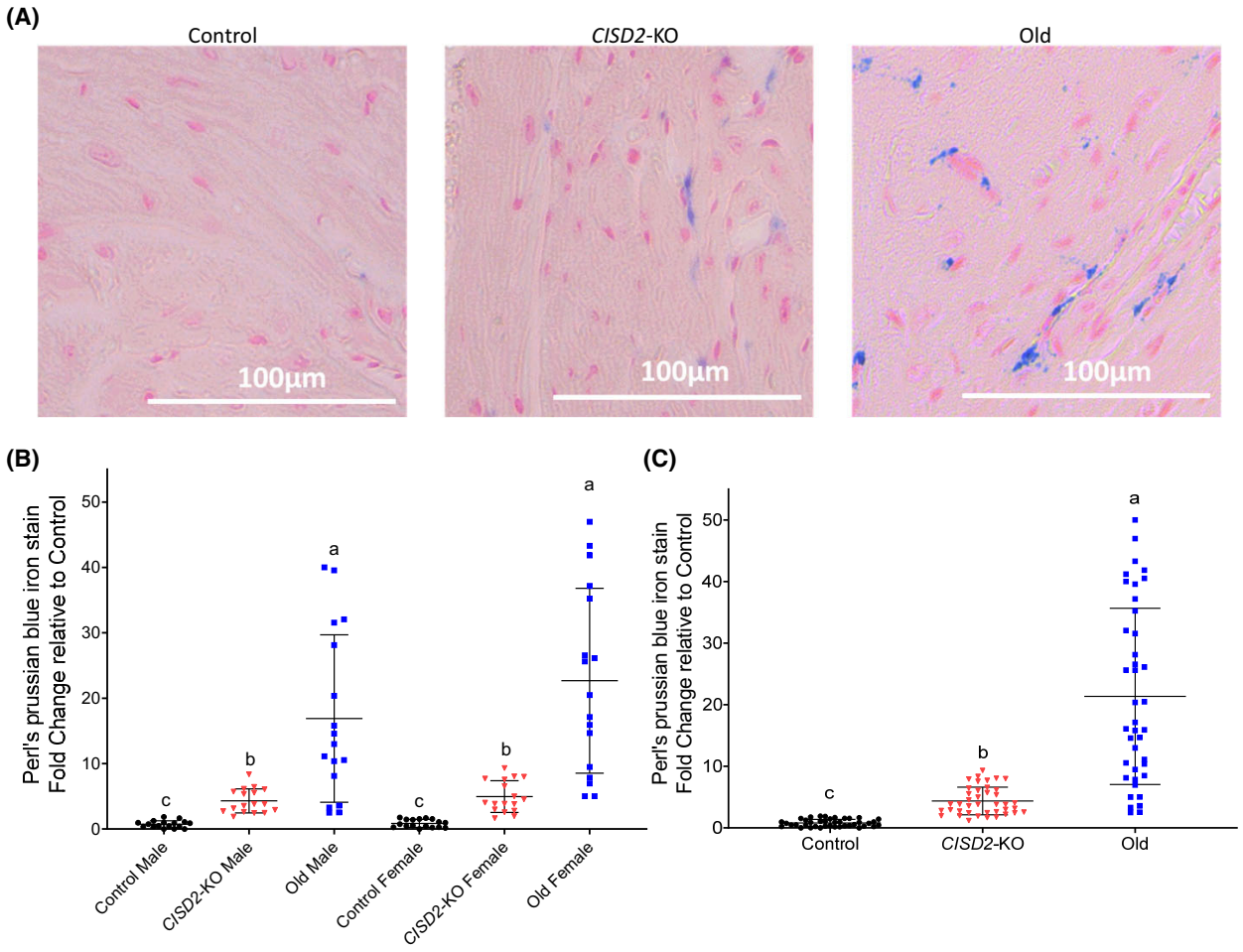


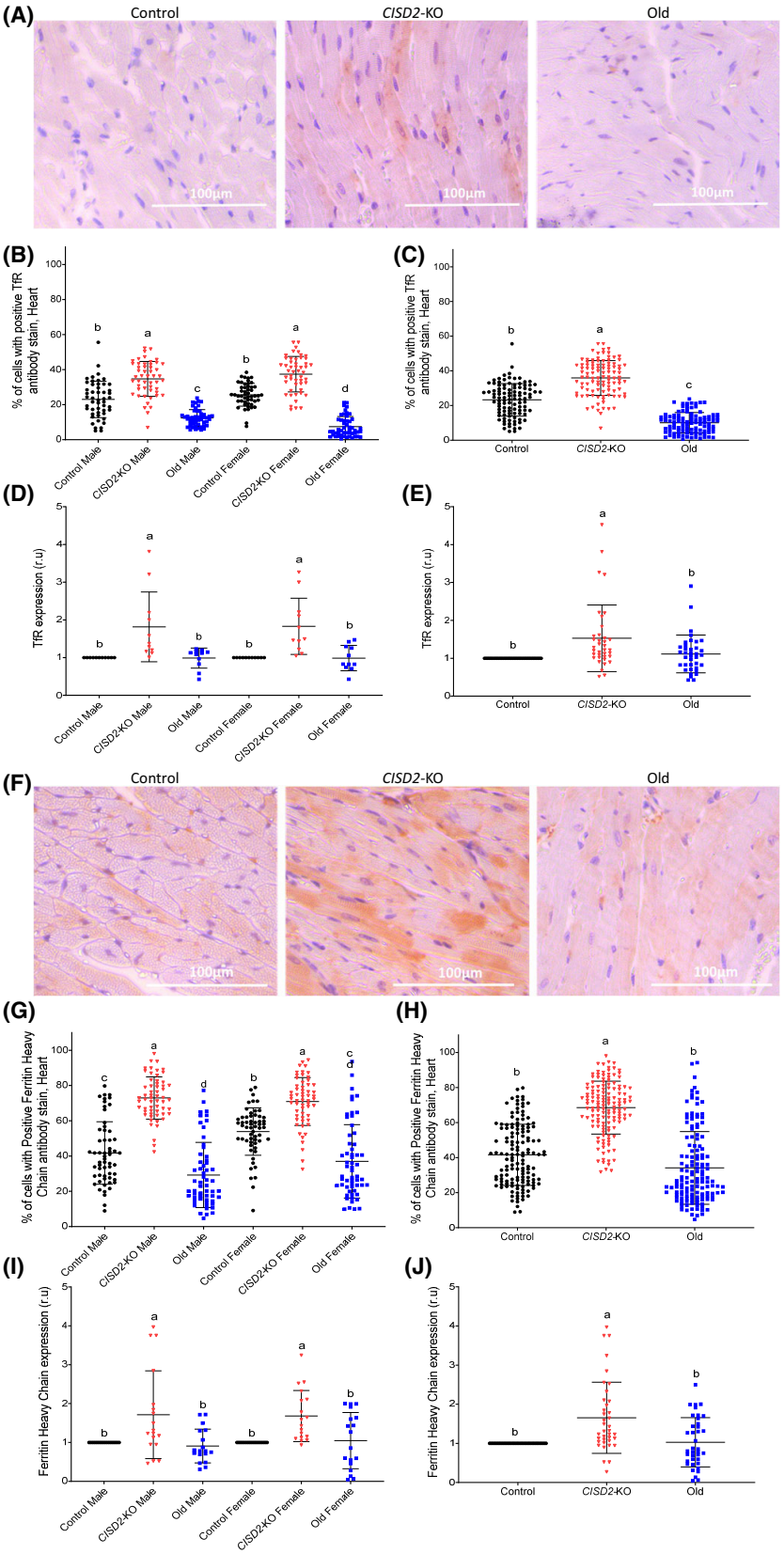
Fig. 2. Accumulation of iron in cardiomyocytes of *CISD2*-KO and old mice. (A) Representative images of heart tissues (left ventricle) from control (22-week-old wild-type), *CISD2*-knockout (KO; 22-week-old *CISD2*-KO), and old (55-week-old wild-type) mice stained for iron content with Perls' Prussian blue. (B, C) Quantitative analysis of Perls' Prussian blue stain in sections from control, *CISD2*-KO, and old mice. Percent (%) of stained cardiomyocytes per field were calculated in each group and compared to control. Results are shown for male and female separately or combined and presented as mean ± SD for six different animals (three different males and three different females) from each group (control, *CISD2*-KO, and old mice). Two-way ANOVA followed by Tukey's test were used to calculate statistical significance. Lowercase letters donate significance ($P < 0.05$).

of *CISD2*-KO mice contained a high number of abnormal ER (altered shape, swollen, and/or fragmented), cardiomyocytes of control or old mice did not (Fig. 4B; male or female).

Our findings that cardiomyocytes of *CISD2*-KO and old mice contained high levels of iron (Fig. 2), as well as abnormal mitochondria (Fig. 4A), but were different in TfR and heavy-chain ferritin expression (Fig. 3), as well as content of damaged ER (Fig. 4B), suggesting that the effects of CISD2 absence on cardiomyocytes of young mice may not fully resemble an accelerated aging process. To further address the

Fig. 3. Expression of TfR and heavy-chain ferritin in cardiomyocytes from *CISD2*-KO and old mice. (A) Representative images of heart tissues (left ventricle) from control (22-week-old wild type), *CISD2*-knockout (KO; 22-week-old *CISD2*-KO), and old (55-week-old wild-type) mice, stained for TfR protein content using IHC. (B, C) Quantitative analysis of TfR protein content in sections from control, *CISD2*-KO, and old mice. Percent (%) of stained cells per field was calculated in each group and compared to control. (D, E) Protein blot analyses of TfR levels in control, *CISD2*-KO, and old mice. (F–J) Same as A to E, but for heavy-chain ferritin. Results are shown for male and female separately or combined and presented as mean ± SD of six different animals (three different males and three different females) from each group (control, *CISD2*-KO, and old mice). Two-way ANOVA followed by Tukey's test were used to calculate statistical significance. Lowercase letters donate significance ($P < 0.05$).

18733468, 2022, 6, Downloaded from https://febs.onlinelibrary.wiley.com/doi/10.1002/1873-3468.14277 by CochraneChina, Wiley Online Library on [02/03/2023]. See the Terms and Conditions (https://onlinelibrary.wiley.com/terms-and-conditions) on Wiley Online Library for rules of use; OA articles are governed by the applicable Creative Commons License



18733468, 2022, 6, Downloaded from https://febs.onlinelibrary.wiley.com/doi/10.1002/1873-3468.14277 by CochraneChina, Wiley Online Library on [02/03/2023]. See the Terms and Conditions (https://onlinelibrary.wiley.com/terms-and-conditions) on Wiley Online Library for rules of use; OA articles are governed by the applicable Creative Commons License

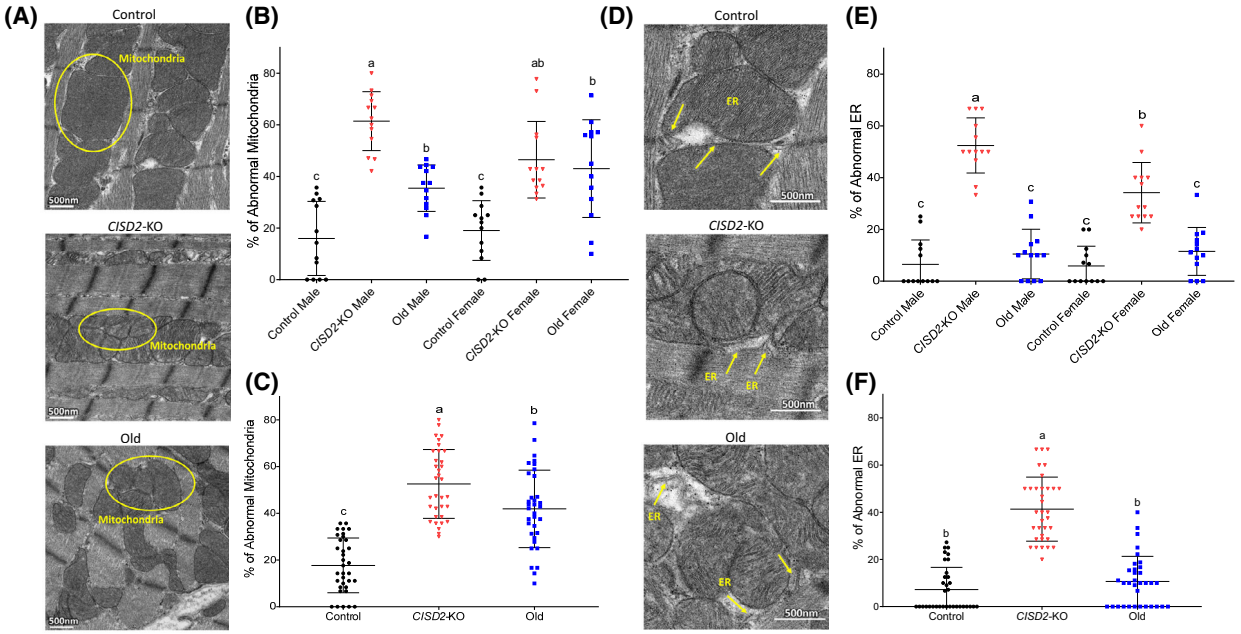


Fig. 4. Enhanced content of damaged mitochondria and ER in cardiomyocytes from *CISD2*-KO mice. (A) Representative transmission electron microscopy images of cardiomyocytes (left ventricle) from control (22-week-old wild-type), *CISD2*-knockout (KO; 22-week-old *CISD2*-KO), and old (55-week-old wild-type) mice, showing damage to mitochondria in cells from *CISD2*-KO and old mice. (B, C) Quantitative analysis of mitochondrial damage in sections from control, *CISD2*-KO, and old mice. Percent (%) of abnormal mitochondria (fewer or disrupted crista and/or abnormal/fragmented shape) per field was calculated in each group and compared to control. (D–F) Same as A to C, but for % of abnormal (altered shape, swollen, and/or fragmented) ER. Results are shown for male and female separately or combined and presented as mean ± SD of six different animals (three different males and three different females) from each group (control, *CISD2*-KO, and old mice). Two-way ANOVA followed by Tukey's test were used to calculate statistical significance. Lowercase letters donate significance ($P < 0.05$).

similarities and differences between hearts subjected to natural aging (old mice) or CISD2 absence (young *CISD2*-KO mice), we conducted proteomics analysis comparing protein abundance between heart tissues from control, *CISD2*-KO, and old mice (Table S2; Fig. 5). The comparison between wild-type young (Control) and old mice hearts revealed a total of 154 proteins with a significant difference in the expression level (up or downregulated; Fig. 5; Table S3). By contrast, the comparison between wild-type young (Control) and *CISD2*-KO mice hearts revealed a total of 69 proteins with significant difference in expression (up or downregulated; Fig. 5; Table S4). Interestingly, an overlap of only 19 proteins was found between these two groups (Fig. 5; Table S5). A comparison of % representation of proteins with different functional and/or biological annotations (Table S6) between the different groups included in our analysis (Fig. 5) revealed that the 19 proteins common to aging and *CISD2* absence included a high representation of proteins involved in oxidative stress, calcium signaling, apoptosis, and ER-related functions. By contrast, the group of 50 proteins unique to *CISD2*-KO contained a high representation of proteins related to mitochondrial function and autophagy, while the group of 135 proteins unique to aging contained a high representation of proteins related to metabolism (Fig. 5; Tables S5 and S6). In addition to these, several proteins involved in the inflammation response (e.g., interleukin enhancer-binding factors 2 and 3) were specifically upregulated in cardiomyocytes from *CISD2*-KO mice, while other proteins involved in inflammation (e.g., protein S100-A8 and -A9, high-mobility group protein B2, and chitinase-like protein 3) were upregulated in cardiomyocytes from both old and *CISD*-KO mice (Table S7).

The availability of proteomics data also allowed us to evaluate the levels of light-chain ferritin in the different tissues. Compared to heavy-chain ferritin, light-chain ferritin was shown to have a much better correlation with cardiac iron levels in mice [53]. As shown in Fig. 6, compared to control young mice or *CISD2*-KO mice, cardiomyocytes of old mice accumulated high levels of light-chain ferritin. This finding suggests that cardiomyocytes of *CISD2*-KO mice have an impaired response to iron overaccumulation (i.e.,

18733468, 2022, 6, Downloaded from https://febs.onlinelibrary.wiley.com/doi/10.1002/1873-3468.14277 by CochraneChina, Wiley Online Library on [02/03/2023]. See the Terms and Conditions (https://onlinelibrary.wiley.com/terms-and-conditions) on Wiley Online Library for rules of use; OA articles are governed by the applicable Creative Commons License

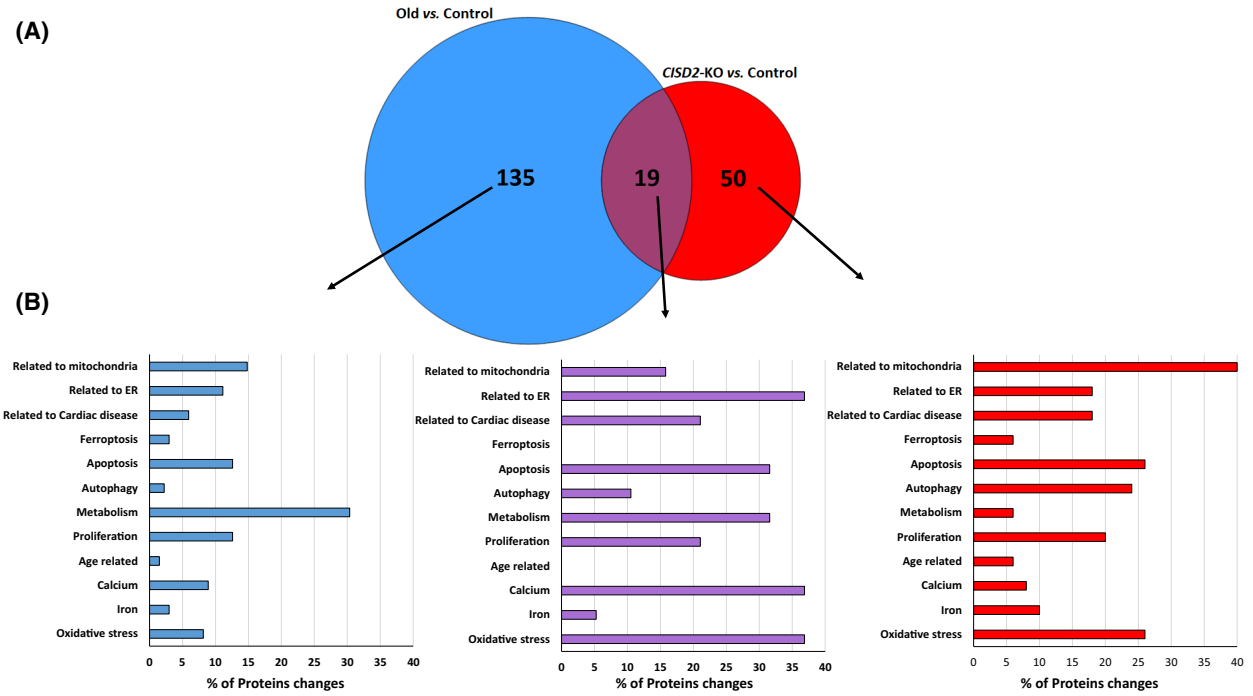


Fig. 5. Proteomics analysis comparing heart tissues from *CISD2*-KO, old, and control mice. (A) Venn Diagram showing the overlap between proteins significantly altered in their expression in heart tissue of old compared to control (blue circle) and *CISD2*-KO compared to control (red circle). Identity of proteins in each group can be found in Table S5. (B) Bar graphs showing the percent (%) representation of proteins belonging to different annotation/function groups (Table S6) in each different section of the Venn diagram shown in A. Proteomics analysis was conducted on heart tissues (left ventricle) obtained from six different animals (three different males and three different females) from each group (control, *CISD2*-KO, and old mice). One-way Welch ANOVA; $N = 18$, $P < 0.05$.

enhanced levels of TfR but not ferritin light-chain; Figs 3 and 6), while cardiomyocytes of old mice respond to iron overaccumulation in a normal way (suppressed TfR and enhanced light-chain ferritin expression; Figs 3 and 6).

Discussion

CISD2 was found to be a key aging gene with ability to slow aging upon overexpression [17,26,27]. With respect to its role in protecting cardiomyocytes from aging, CISD2 was proposed to prevent age-related alterations in calcium homeostasis that would cause impaired electromechanical functioning, mitochondrial dysfunction, and tissue damage [17,27]. Although CISD2 was shown to protect different cells from over-accumulation of mitochondrial iron [16,54,55], its role in protecting cardiomyocytes from age-related iron accumulation [13,14,27,56] was not demonstrated previously. Here, we reveal that in the absence of CISD2, cardiomyocytes accumulate high levels of iron (Fig. 2). Interestingly, although cardiomyocytes from old mice also accumulate high levels of iron (Fig. 2), our findings suggest that they may be accumulating these high levels of iron over a longer time period, potentially using a different mechanism than that found in young *CISD2*-KO cells. This possibility is supported by our findings that cardiomyocytes of young *CISD2*-KO mice display enhanced expression of TfR and heavy-chain ferritin (but not light chain ferritin), while cardiomyocytes from old mice display suppressed levels of TfR and enhanced levels of light-chain ferritin (Figs 3 and 6). It is possible, of course, that over time, the age-related decline in CISD2 protein levels (Fig. 1; [27]) is driving the accumulation of iron in aging cardiomyocytes and that this process is accompanied by elevated expression of TfR (that subsides by 55 weeks of age). In contrast, the absence of CISD2 in cardiomyocytes from young mice could drive an active process of iron uptake, similar to the processes observed in different cells upon iron starvation, or in cancer cells that actively accumulate iron [16,17,37,52,57,58]. Because we did not analyze the expression of TfR and ferritins in cardiomyocytes during different stages of the aging process, we cannot determine whether the mechanisms of iron

18733468, 2022, 6, Downloaded from https://febs.onlinelibrary.wiley.com/doi/10.1002/1873-3468.14277 by CochraneChina, Wiley Online Library on [02/03/2023]. See the Terms and Conditions (https://onlinelibrary.wiley.com/terms-and-conditions) on Wiley Online Library for rules of use; OA articles are governed by the applicable Creative Commons License

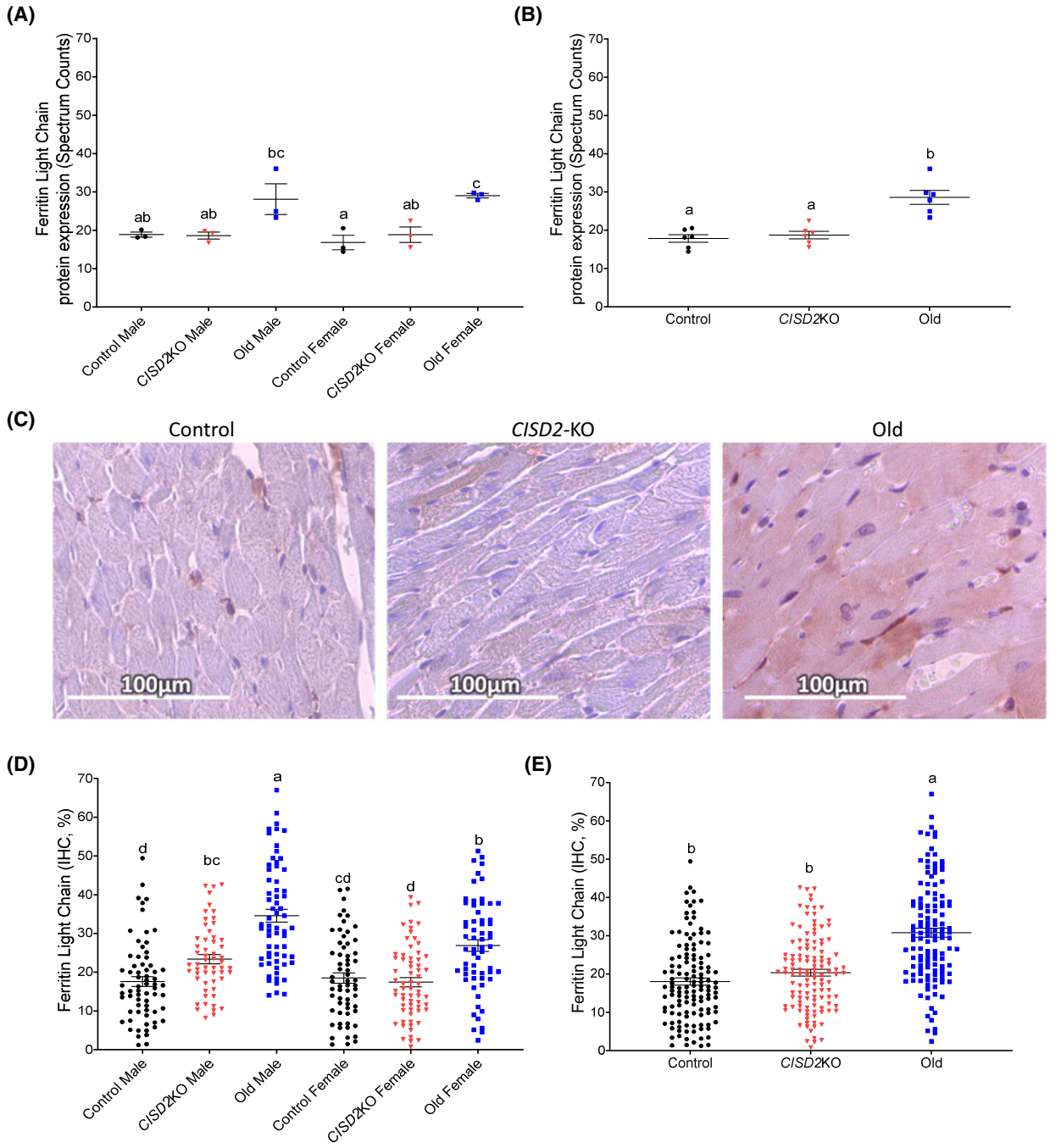


Fig. 6. Expression of light-chain ferritin in cardiomyocytes from *CISD2*-KO and old mice. (A, B) Proteomics analyses of light-chain ferritin levels in control, *CISD2*-KO, and old mice. (C) Representative images of heart tissues (left ventricle) from control (22-week-old wild-type), *CISD2*-knockout (KO; 22-week-old *CISD2*-KO), and old (55-week-old wild-type) mice, stained for light-chain ferritin protein content using IHC. (D, E) Quantitative analysis of light-chain ferritin protein content in sections from control, *CISD2*-KO, and old mice. Percent (%) of stained cells per field was calculated in each group and compared to control. Results are shown for male and female separately or combined and presented as mean ± SD of six different animals (three different males and three different females) from each group (control, *CISD2*-KO, and old mice). Two-way ANOVA followed by Tukey's test were used to calculate statistical significance. Lowercase letters donate significance ($P < 0.05$).

18733468, 2022, 6, Downloaded from https://febs.onlinelibrary.wiley.com/doi/10.1002/1873-3468.14277 by CochraneChina, Wiley Online Library on [02/03/2023]. See the Terms and Conditions (https://onlinelibrary.wiley.com/terms-and-conditions) on Wiley Online Library for rules of use; OA articles are governed by the applicable Creative Commons License

accumulation found in cardiomyocytes from old and young *CISD2*-KO mice are similar. In general, as described above, the regulation of iron levels in cardiomyocytes from *CISD2*-KO mice appears to be disrupted (Figs 2, 3 and 6). Although it is unknown at present what is the mechanism underlying this disruption, the findings that CISD1 can repair the oxidatively damaged Fe–S clusters of iron regulatory protein 1 (IRP1) [59], that CISD1 and CISD2 cooperate in regulating iron levels in cells [32], and that IRP regulates the expression level of TfR [60] may suggest that disrupting CISD2 function (i.e., *CISD2*-KO) could result in aberrant expression of TfR, even when high levels of iron accumulate in cells. Further studies are needed to address the mechanisms of iron regulation mediated by CISD2 in cells.

Interestingly, one of the proteins identified by our proteomics analysis as induced in cardiomyocytes from old mice, as well as in cardiomyocytes from young *CISD2*-KO mice, is glycogen synthase kinase 3β (Gsk3β; among the 19 proteins common to Old and *CISD2*-KO mice in Fig. 5; Table S5). Glycogen synthase kinase 3β was previously found to be involved in regulating iron uptake into cells *via* promoting the enhanced endocytosis of transferrin-loaded vesicles [61,62]. The accumulation of Gsk3β in cardiomyocytes of old and young *CISD2*-KO mice could suggest that the high levels of iron observed in these cells (Fig. 2) is mediated, at least, in part, by Gsk3β-enhanced endocytosis of transferrin into cells. Further studies are needed to substantiate this possibility.

Previous studies revealed that different cell types with reduced *CISD2* or *CISD1* expression accumulate high levels of iron in their mitochondria and display enhanced expression of TfR and ferritin [54,58,63]. This process is also accompanied by the activation of apoptosis, autophagy, and ferroptosis [16,33,50,54,57,58,64,65]. The similarities observed between cells with suppressed *CISD2* or *CISD1* expression led to the hypothesis that these two proteins participate in similar or overlapping processes [16,32,54]. Indeed, CISD1 was found to interact with CISD2 and donate its clusters to it [32], and the role of the CISD2 clusters was found to be critical for cellular protection from iron and ROS overload, as well as for the activation of apoptosis and/or ferroptosis [16,54,55]. *CISD1* was recently found to protect the mitochondria of mice cardiomyocytes from overaccumulation of iron and ROS [28]. Because CISD1 and CISD2 cooperate in the protection of cancer and insulinoma cells from enhanced accumulation of iron and ROS [32,39,50], it is possible that they are also cooperating in this process in cardiomyocytes (Fig. 7).

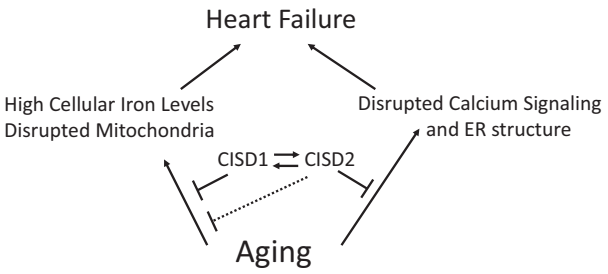


Fig. 7. A model showing the possible interactions between *CISD2* and *CISD1* in cardiomyocytes, preventing HF. *CISD2* is shown to prevent alterations in calcium homeostasis/signaling, damage to mitochondria, and damage to the ER. *CISD2* is also shown to prevent, either directly or through *CISD1*, the accumulation of iron in heart cells. The model is based on findings presented in this study as well as in Refs [27,28] and suggests that *CISD2* and *CISD1* could be playing a coordinated role in protecting the heart from aging and HF.

Thus, although the CISD1 protein is present in cardiomyocytes of *CISD2*-KO mice (Fig. 1), it is unable to conduct its function in the absence of CISD2 [16,17,27]. Further studies are needed to address the potential interactions between CISD1 and CISD2 in cardiomyocytes.

In addition to differences in TfR, light-, and heavy-chain ferritin expression between cardiomyocytes from old and young *CISD2*-KO mice (Figs 3 and 6), our study identified differences in structural damage to the ER (Fig. 4) and differences in protein expression patterns (Fig. 5) between these two treatment groups. Taken together, the lack of *CISD2* appears, therefore, to resemble some aspects of the normal aging process related to mitochondrial dysfunction, iron accumulation, and expression of proteins associated with calcium, oxidative stress, and ER functions. However, as reflected in the proteomics analysis, there were more old- or *CISD2*-KO-specific proteins than proteins shared between old and *CISD2*-KO (Fig. 5). *CISD2* could, therefore, protect cardiomyocytes from certain aspects of aging, but not all. Further studies are, of course, needed to address the role of *CISD2* in the aging process of the heart. In particular, a detailed time-course of molecular, metabolic, and proteomic changes in cardiomyocytes from control and *CISD2*-KO mice during aging is provided. As proposed in the model presented in Fig. 7 (based on our results as well as previous publications [27,28]), *CISD2* may have specific (e.g., protection of ER and calcium homeostasis) or *CISD1*-shared (e.g., protection of mitochondria and iron homeostasis) functions during aging.

18733468, 2022, 6, Downloaded from https://febs.onlinelibrary.wiley.com/doi/10.1002/1873-3468.14277 by CochraneChina, Wiley Online Library on [02/03/2023]. See the Terms and Conditions (https://onlinelibrary.wiley.com/terms-and-conditions) on Wiley Online Library for rules of use; OA articles are governed by the applicable Creative Commons License

Acknowledgements

OK acknowledges The Annual Golda Meir Fellowship and The Hebrew University Rector for the Emergency Scholarship recipients for Postdoctoral fellows, 2020–2021. This study was supported by the National Science Foundation (NSF)-Binational Science Foundation (BSF) Grant NSF-MCB 1613462 (to RM) and BSF Grant 2015831 (to RN), as well as by GM111364 (to RM). We would also like to acknowledge the Charles W. Gehrke Proteomics and Electron Microscopy Research Core Facilities, as well as the Veterinary Diagnostic Laboratory at the University of Missouri, Columbia.

Data accessibility

Proteomics data were deposited in Pride (https://www.ebi.ac.uk/pride/), under the following accession number: PXD028367.

Author contributions

RN, RM, and CM-A involved in the conceptualization. OK, LR, RN, CM-A, and RM designed the experiment. OK, LR, and SDK collected the data. OK, SDK, and LR involved in the methodology. OK involved in the data curation. OK and LR analyzed the data formally. RM and RN acquired the funding. OK, LR, RN, CM-A, IZC, and RM wrote the manuscript.

References

1 Oneglia A, Nelson MD, Merz CNB. Sex differences in cardiovascular aging and heart failure. *Curr Heart Fail Rep*. 2020;**17**:409–23.
2 North BJ, Sinclair DA. The intersection between aging and cardiovascular disease. *Circ Res*. 2012;**110**:1097–108.
3 López-Otín C, Blasco MA, Partridge L, Serrano M, Kroemer G. The hallmarks of aging. *Cell*. 2013;**153**:1194–217.
4 Aimo A, Castiglione V, Borrelli C, Saccaro LF, Franzini M, Masi S, et al. Oxidative stress and inflammation in the evolution of heart failure: from pathophysiology to therapeutic strategies. *Eur J Prev Cardiol*. 2020;**27**:494–510.
5 Li H, Hastings MH, Rhee J, Trager LE, Roh JD, Rosenzweig A. Targeting age-related pathways in heart failure. *Circ Res*. 2020;**126**:533–51.
6 Javadov S, Kozlov AV, Camara AK. Mitochondria in health and diseases. *Cells*. 2020;**9**:1177–86.
7 Faizan MI, Ahmad T. Altered mitochondrial calcium handling and cell death by necroptosis: an emerging paradigm. *Mitochondrion*. 2021;**57**:47–62.
8 Rottenberg H, Hoek JB. The mitochondrial permeability transition: nexus of aging, disease and longevity. *Cells*. 2021;**10**:79–102.
9 Srivastava S. The mitochondrial basis of aging and age-related disorders. *Genes*. 2017;**8**:398–421.
10 Liu YJ, McIntyre RL, Janssens GE, Houtkooper RH. Mitochondrial fission and fusion: a dynamic role in aging and potential target for age-related disease. *Mech Ageing Dev*. 2020;**186**:111212–25.
11 Picca A, Mankowski RT, Burman JL, Donisi L, Kim J-S, Marzetti E, et al. Mitochondrial quality control mechanisms as molecular targets in cardiac ageing. *Nat Rev Cardiol*. 2018;**15**:543–54.
12 Chen Q, Samidurai A, Thompson J, Hu Y, Das A, Willard B, et al. Endoplasmic reticulum stress-mediated mitochondrial dysfunction in aged hearts. *Biochim Biophys Acta Mol Basis Dis*. 2020;**1866**:165899–913.
13 Quan Y, Xin Y, Tian G, Zhou J, Liu X. Mitochondrial ROS-modulated mtDNA: a potential target for cardiac aging. *Oxid Med Cell Longev*. 2020;**2020**:1–11.
14 Wofford JD, Chakrabarti M, Lindahl PA. Mössbauer spectra of mouse hearts reveal age-dependent changes in mitochondrial and ferritin iron levels. *J Biol Chem*. 2017;**292**:5546–54.
15 Karmi O, Marjault H-B, Pesce L, Carloni P, Onuchic JN, Jennings PA, et al. The unique fold and lability of the [2Fe-2S] clusters of NEET proteins mediate their key functions in health and disease. *J Biol Inorg Chem*. 2018;**23**:599–612.
16 Nechushtai R, Karmi O, Zuo K, Marjault H-B, Darash-Yahana M, Sohn Y-S, et al. The balancing act of NEET proteins: iron, ROS, calcium and metabolism. *Biochim Biophys Acta Mol Cell Res*. 2020;**1867**:118805–22.
17 Shen Z-Q, Huang Y-L, Teng Y-C, Wang T-W, Kao C-H, Yeh C-H, et al. CISD2 maintains cellular homeostasis. *Biochim Biophys Acta Mol Cell Res*. 2021;**1868**:118954–70.
18 Amr S, Heisey C, Zhang M, Xia XJ, Shows KH, Ajlouni K, et al. A homozygous mutation in a novel zinc-finger protein, ERIS, is responsible for Wolfram syndrome 2. *Am J Hum Genet*. 2007;**81**:673–83.
19 Mozzillo E, Delvecchio M, Carella M, Grandone E, Palumbo P, Salina A, et al. A novel CISD2 intragenic deletion, optic neuropathy and platelet aggregation defect in Wolfram syndrome type 2. *Bmc Med Genet*. 2014;**15**:1–7.
20 Rondinelli M, Novara F, Calcaterra V, Zuffardi O, Genovese S. Wolfram syndrome 2: a novel CISD2 mutation identified in Italian siblings. *Acta Diabetol*. 2015;**52**:175–8.

18733468, 2022, 6, Downloaded from https://febs.onlinelibrary.wiley.com/doi/10.1002/1873-3468.14277 by CochraneChina, Wiley Online Library on [02/03/2023]. See the Terms and Conditions (https://onlinelibrary.wiley.com/terms-and-conditions) on Wiley Online Library for rules of use; OA articles are governed by the applicable Creative Commons License

21 Rouzier C, Moore D, Delorme C, Lacas-Gervais S, Ait-El-Mkadem S, Fragaki K, et al. A novel CISD2 mutation associated with a classical Wolfram syndrome phenotype alters Ca2+ homeostasis and ER-mitochondria interactions. *Hum Mol Genet*. 2017;**26**:1599–611.
22 Akturk HK, Yasa S. Previously unreported abnormalities in Wolfram syndrome type 2. *Pediatr Endocrinol Diabetes Metab*. 2017;**23**:107–10.
23 Pourreza MR, Sobhani M, Rahimi A, Aramideh M, Kajbafzadeh AM, Noori-Daloii MR, et al. Homozygosity mapping and direct sequencing identify a novel pathogenic variant in the CISD2 gene in an Iranian Wolfram syndrome family. *Acta Diabetol*. 2020;**57**:81–7.
24 Chen YF, Kao CH, Chen YT, Wang CH, Wu CY, Tsai CY, et al. Cisd2 deficiency drives premature aging and causes mitochondria-mediated defects in mice. *Genes Dev*. 2009;**23**:1183–94.
25 Chen YF, Wu CY, Kirby R, Kao CH, Tsai TF. A role for the CISD2 gene in lifespan control and human disease. *Ann N Y Acad Sci*. 2010;**1201**:58–64.
26 Wu CY, Chen YF, Wang CH, Kao CH, Zhuang HW, Chen CC, et al. A persistent level of Cisd2 extends healthy lifespan and delays aging in mice. *Hum Mol Genet*. 2012;**21**:3956–68.
27 Yeh CH, Shen ZQ, Hsiung SY, Wu PC, Teng YC, Chou YJ, et al. Cisd2 is essential to delaying cardiac aging and to maintaining heart functions. *PLoS Biol*. 2019;**17**:e3000508.
28 Furihata T, Takada S, Kakutani N, Maekawa S, Tsuda M, Matsumoto J, et al. Cardiac-specific loss of mitoNEET expression is linked with age-related heart failure. *Commun Biol*. 2021;**4**:138–49.
29 Hua J, Gao Z, Zhong S, Wei B, Zhu J, Ying R. CISD1 protects against atherosclerosis by suppressing lipid accumulation and inflammation via mediating Drp1. *Biochem Biophys Res Comm*. 2021;**577**:80–8.
30 Ferecatu I, Goncalves S, Golinelli-Cohen MP, Clemancey M, Martelli A, Riquier S, et al. The diabetes drug target MitoNEET governs a novel trafficking pathway to rebuild an Fe-S cluster into cytosolic aconitase/iron regulatory protein 1. *J Biol Chem*. 2014;**289**:28070–86.
31 Tan G, Liu D, Pan F, Zhao J, Li T, Ma Y, et al. His-87 ligand in mitoNEET is crucial for the transfer of iron sulfur clusters from mitochondria to cytosolic aconitase. *Biochem Biophys Res Commun*. 2016;**470**:226–32.
32 Karmi O, Holt SH, Song L, Tamir S, Luo Y, Bai F, et al. Interactions between mitoNEET and NAF-1 in cells. *PLoS One*. 2017;**12**:e0175796.
33 Yuan H, Li X, Zhang X, Kang R, Tang D. CISD1 inhibits ferroptosis by protection against mitochondrial lipid peroxidation. *Biochem Biophys Res Commun*. 2016;**478**:838–44.
34 Geldenhuys WJ, Benkovic SA, Lin L, Yonutas HM, Crish SD, Sullivan PG, et al. MitoNEET (CISD1) knockout mice show signs of striatal mitochondrial dysfunction and a Parkinson's disease phenotype. *ACS Chem Neurosci*. 2017;**8**:2759–65.
35 Yonutas HM, Hubbard WB, Pandya JD, Vekaria HJ, Geldenhuys WJ, Sullivan PG. Bioenergetic restoration and neuroprotection after therapeutic targeting of mitoNEET: new mechanism of pioglitazone following traumatic brain injury. *Exp Neurol*. 2020;**327**:113243–54.
36 Stauch KL, Villeneuve LM, Totusek S, Lamberty B, Ciborowski P, Fox HS. Quantitative proteomics of presynaptic mitochondria reveal an overexpression and biological relevance of neuronal MitoNEET in postnatal brain development. *Dev Neurobiol*. 2019;**79**:370–86.
37 Tamir S, Paddock ML, Darash-Yahana-Baram M, Holt SH, Sohn YS, Agranat L, et al. Structure-function analysis of NEET proteins uncovers their role as key regulators of iron and ROS homeostasis in health and disease. *Biochim Biophys Acta*. 2015;**1853**:1294–315.
38 Holt SH, Darash-Yahana M, Sohn YS, Song L, Karmi O, Tamir S, et al. Activation of apoptosis in NAF-1-deficient human epithelial breast cancer cells. *J Cell Sci*. 2016;**129**:155–65.
39 Sohn YS, Tamir S, Song L, Michaeli D, Matouk I, Conlan AR, et al. NAF-1 and mitoNEET are central to human breast cancer proliferation by maintaining mitochondrial homeostasis and promoting tumor growth. *Proc Natl Acad Sci USA*. 2013;**110**:14676–81.
40 Danielpur L, Sohn YS, Karmi O, Fogel C, Zinger A, Abu-Libdeh A, et al. GLP-1-RA corrects mitochondrial labile iron accumulation and improves beta-cell function in type 2 Wolfram syndrome. *J Clin Endocrinol Metab*. 2016;**101**:3592–9.
41 Fishbein MC, Wang T, Matijasevic M, Hong L, Apple FS. Myocardial tissue troponins T and I: an immunohistochemical study in experimental models of myocardial ischemia. *Cardiovasc Pathol*. 2003;**12**:65–71.
42 Shi S-R, Key ME, Kalra KL. Antigen retrieval in formalin-fixed, paraffin-embedded tissues: an enhancement method for immunohistochemical staining based on microwave oven heating of tissue sections. *J Histochem Cytochem*. 1991;**39**:741–8.
43 Gössl M, Versari D, Hildebrandt HA, Bajanowski T, Sangiorgi G, Erbel R, et al. Segmental heterogeneity of vasa vasorum neovascularization in human coronary atherosclerosis. *JACC Cardiovasc Imaging*. 2010;**3**:32–40.
44 Pan X, Sands SA, Yue Y, Zhang K, LeVine SM, Duan D. An engineered galactosylceramidase construct

18733468, 2022, 6, Downloaded from https://febs.onlinelibrary.wiley.com/doi/10.1002/1873-3468.14277 by CochraneChina, Wiley Online Library on [02/03/2023]. See the Terms and Conditions (https://onlinelibrary.wiley.com/terms-and-conditions) on Wiley Online Library for rules of use; OA articles are governed by the applicable Creative Commons License

improves AAV gene therapy for Krabbe disease in Twitcher mice. *Hum Gene Ther*. 2019;**30**:1039–51.
45 Zandalinas SI, Song L, Sengupta S, McInturf SA, Grant DG, Marjault H-B, et al. Expression of a dominant-negative AtNEET-H89C protein disrupts iron–sulfur metabolism and iron homeostasis in Arabidopsis. *Plant J*. 2020;**101**:1152–69.
46 Yang BO, Li R, Liu PN, Geng X, Mooney BP, Chen C, et al. Quantitative proteomics reveals docosahexaenoic acid-mediated neuroprotective effects in lipopolysaccharide-stimulated microglial cells. *J Proteome Res*. 2020;**19**:2236–46.
47 Karmi O, Sohn Y-S, Zandalinas SI, Rowland L, King S, Nechushtai R, et al. Disrupting CISD2 function in cancer cells primarily impacts mitochondrial labile iron levels and triggers TXNIP expression. *Free Radic Biol Med*. 2021;**176**:92–104.
48 Gammella E, Buratti P, Cairo G, Recalcati S. The transferrin receptor: the cellular iron gate. *Metallomics*. 2017;**9**:1367–75.
49 Arosio P, Elia L, Poli M. Ferritin, cellular iron storage and regulation. *IUBMB Life*. 2017;**69**:414–22.
50 Karmi O, Sohn Y-S, Marjault H-B, Israeli T, Leibowitz G, Ioannidis K, et al. A combined drug treatment that reduces mitochondrial iron and reactive oxygen levels recovers insulin secretion in NAF-1-deficient pancreatic cells. *Antioxidants*. 2021;**10**:1160–79.
51 Shen Z-Q, Chen Y-F, Chen J-R, Jou Y-S, Wu P-C, Kao C-H, et al. CISD2 haploinsufficiency disrupts calcium homeostasis, causes nonalcoholic fatty liver disease, and promotes hepatocellular carcinoma. *Cell Rep*. 2017;**21**:2198–211.
52 Mittler R, Darash-Yahana M, Sohn YS, Bai F, Song L, Cabantchik IZ, et al. A new link between iron metabolism, reactive oxygen species, and cancer. *Antioxid Redox Signal*. 2019;**30**:1083–95.
53 Brewer CJ, Wood RI, Wood JC. mRNA regulation of cardiac iron transporters and ferritin subunits in a mouse model of iron overload. *Exp Hematol*. 2014;**42**:1059–67.
54 Mittler R, Darash-Yahana M, Sohn YS, Bai F, Song L, Cabantchik IZ, et al. NEET proteins: a new link between iron metabolism, reactive oxygen species, and cancer. *Antioxid Redox Signal*. 2019;**30**:1083–95.
55 Darash-Yahana M, Pozniak Y, Lu M, Sohn YS, Karmi O, Tamir S, et al. Breast cancer tumorigenicity is dependent on high expression levels of NAF-1 and the lability of its Fe-S clusters. *Proc Natl Acad Sci USA*. 2016;**113**:10890–5.
56 Kumar V, Kumar TS, Kartha C. Mitochondrial membrane transporters and metabolic switch in heart failure. *Heart Fail Rev*. 2019;**24**:255–67.
57 Kim EH, Shin D, Lee J, Jung AR, Roh J-L. CISD2 inhibition overcomes resistance to sulfasalazine-induced ferroptotic cell death in head and neck cancer. *Cancer Lett*. 2018;**432**:180–90.
58 Shao F, Du J, Li Y, Yu J, Wu H, Ying K. Downregulation of CISD2 has prognostic value in non-small cell lung cancer and inhibits the tumorigenesis by inducing mitochondrial dysfunction. *Front Oncol*. 2020;**10**:3187–99.
59 Ferecatu I, Gonçalves S, Golinelli-Cohen MP, Clémancey M, Martelli A, Riquier S, et al. The diabetes drug target MitoNEET governs a novel trafficking pathway to rebuild an Fe-S cluster into cytosolic aconitase/iron regulatory protein 1. *J Biol Chem*. 2014;**289**:28070–86.
60 Huynh N, Ou Q, Cox P, Lill R, King-Jones K. Glycogen branching enzyme controls cellular iron homeostasis via iron regulatory protein 1 and mitoNEET. *Nat Commun*. 2019;**10**:5463.
61 Anzovino A, Chiang S, Brown BE, Hawkins CL, Richardson DR, Huang ML-H. Molecular alterations in a mouse cardiac model of Friedreich ataxia: an impaired Nrf2 response mediated via upregulation of Keap1 and activation of the Gsk3β axis. *Am J Pathol*. 2017;**187**:2858–75.
62 Guyett PJ, Xia S, Swinney DC, Pollastri MP, Mensa-Wilmot K. Glycogen synthase kinase 3β promotes the endocytosis of transferrin in the African trypanosome. *ACS Infect Dis*. 2016;**2**:518–28.
63 Furihata T, Takada S, Maekawa S, Mizushima W, Watanabe M, Takahashi H, et al. mitoNEET regulates mitochondrial iron homeostasis interacting with transferrin receptor. *bioRxiv*. 2018;330084 [PREPRINT].
64 Homma T, Kobayashi S, Fujii J. Cysteine preservation confers resistance to glutathione-depleted cells against ferroptosis via CDGSH iron sulphur domain-containing proteins (CISDs). *Free Radical Res*. 2020;**54**:397–407.
65 Hassannia B, Van Coillie S, Vanden Berghe T. Ferroptosis: biological rust of lipid membranes. *Antioxid Redox Signal*. 2021;**35**:487–509.

Supporting information

Additional supporting information may be found online in the Supporting Information section at the end of the article.

Fig. S1. PCR analysis of transgenic mice.

Fig. S2. Expression of the three human NEET proteins (CISD1, 2, and 3) in the human heart.

Table S1. Analysis of blood samples from the different mice used for this study.

Table S2. Proteins significantly altered in their expression between heart tissues from control, *CISD2*-KO, and old mice.

18733468, 2022, 6, Downloaded from https://febs.onlinelibrary.wiley.com/doi/10.1002/1873-3468.14277 by CochraneChina, Wiley Online Library on [02/03/2023]. See the Terms and Conditions (https://onlinelibrary.wiley.com/terms-and-conditions) on Wiley Online Library for rules of use; OA articles are governed by the applicable Creative Commons License

Table S3. Proteins significantly altered in their expression between wild-type young (control) and old mice hearts.
Table S4. Proteins significantly altered in their expression between wild-type young (control) and *CISD2*-KO mice hearts.
Table S5. Identity of proteins shown in the different sections of the Venn diagram presented in Fig. 5A.
Table S6. List of all proteins belonging to each of the functional annotation groups presented in Figure 5B.
Table S7. List of proteins involved in the inflammatory response identified by the proteomics analysis.

18733468, 2022, 6, Downloaded from https://febs.onlinelibrary.wiley.com/doi/10.1002/1873-3468.14277 by CochraneChina, Wiley Online Library on [02/03/2023]. See the Terms and Conditions (https://onlinelibrary.wiley.com/terms-and-conditions) on Wiley Online Library for rules of use; OA articles are governed by the applicable Creative Commons License